HHS Public Access

Author manuscript

Nat Biomed Eng. Author manuscript; available in PMC 2018 January 18.

Published in final edited form as:

Nat Biomed Eng. 2017 ; 1: . doi:10.1038/s41551-017-0080.

A Fully Functional Drug-Eluting Joint Implant

VJ Suhardi[1,2,3], **DA Bichara**[1,2], **SJJ Kwok**[3,4], **AA Freiberg**[2], **H Rubash**[2], **H Malchau**[2], **SH Yun**[3,4], **OK Muratoglu**[1,2], and **E Oral**[1,2]

[1]Harris Orthopaedic Laboratory, Massachusetts General Hospital, Boston, MA

[2]Department of Orthopaedic Surgery, Harvard Medical School

[3]Department of Medical Engineering and Medical Physics, Massachusetts Institute of Technology

[4]Wellmann Center for Photomedicine, Massachusetts General Hospital, Boston, MA

Abstract

Despite advances in orthopedic materials, the development of drug-eluting bone and joint implants that can sustain the delivery of the drug and maintain the necessary mechanical strength in order to withstand loading has remained elusive. Here, we demonstrate that modifying the eccentricity of drug clusters and the percolation threshold in ultrahigh molecular weight polyethylene (UHMWPE) results in maximized drug elution and in the retention of mechanical strength. The optimized UHMWPE eluted antibiotic at a higher concentration for longer than the clinical gold standard antibiotic-eluting bone cement while retaining the mechanical and wear properties of clinically used UHMWPE joint prostheses. Treatment of lapine knees infected with *Staphylococcus aureus* with the antibiotic-eluting UHMWPE led to complete bacterial eradication and to the absence of detectable systemic effects. We argue that the antibiotic-eluting UHMWPE joint implant is a promising candidate for clinical trials.

More than one million joint replacements are performed annually in the U.S [1]. Five to ten percent of joint replacements are revised within seven years [2] with prosthetic joint infection (PJI) being one of the most common reasons for revision [3]. PJI is an increasing healthcare burden [4] with a recurrence rate of 16 % [5]) and a mortality rate of 2.5 % [6]. End-stage treatments are severely morbid, including multiple revisions, resection arthroplasty, arthrodesis and amputation [7].

Correspondence to: E Oral.

Author contributions

J.S., D.A.B, E.O, O.K.M, R.H, F.A, M.H., S.K, and Y.H. designed the experiments. J.S., D.A.B., and S.K. performed the experiments. All the authors were involved in the analyses and interpretation of the data. J.S., D.A.B, S.K., E.O, and O.K.M wrote the paper, with the help of the co-authors.

Supplementary information is available for this paper

Competing financial interests

The authors declare no competing financial interests.

Antibiotic penetration into the joint space and bone from systemic administration is limited because of poor blood supply to the infected area [8]. A strategy to address this is to deliver antibiotics locally by incorporating them into orthopaedic implant materials [9, 10]. The current treatments incorporate antibiotics into poly methyl-methacrylate bone cement [10], ceramic bone graft substitutes [11], or resorbable polymeric systems [12]. The gold standard in treating PJI involves two-stage surgery where removal of all components of the infected implants is followed by a minimum of 6–8 weeks of antibiotic-eluting bone cement (BC) spacer placement where the patients have limited mobility and function ([13]; Figure 1). This period is followed by the placement of new implant components; but in cases where the temporary spacers are used for long-term weight bearing without the placement of new implants, BC spacers have shown a complication rate of 26–60 % within 49–54 months [14], mainly due to dislocation (11–17 %) and fracture (10–14 %). The primary use of BC in joint implants is fixation of the bone-implant interface; however, BC has low tensile strength and impact toughness [15, 16] and is unsuitable for use in continuous load-bearing [17, 18].

The high incidence of BC fractures (Figure 1; [14]) is also due to the decrease in mechanical properties caused by incorporated antibiotics [19]. In addition, while drug elution into the peri-prosthetic space is desired for 3–8 weeks, the elution from antibiotic-eluting BC spacers often falls below the minimum inhibitory concentration (MIC) of common PJI bacterial contaminants within 1 week [20]. Low antibiotic concentration without complete eradication of bacteria has the potential of increasing antibiotic resistance [21]. The antibiotic concentration in BC is limited by the minimum allowed mechanical properties, but results in low interconnectivity of drug clusters (Figure 1; [22]). In fact, for drug-eluting polymers with spherical drug clusters [23], it has been shown that 40–60 % (w/w) drug content is required to reach complete interconnectivity. Our goal was to develop load-bearing joint implant materials with efficient antibiotic release for at least 3 weeks and high mechanical strength and wear resistance within that of clinically used UHMWPE (Supplementary Discussion 1), to allow direct replacement of infected prosthetics with a new implant (Figure 1) without the complications and morbidity associated with a two-stage procedure.

Drug cluster interconnectivity was studied using percolation theory, which showed that drug elution increased sharply as the percolation threshold was reached [24], whereas mechanical strength decreased with total drug content [25]. Computational simulation showed further that increasing eccentricity of the drug cluster shape [26] and increasing polymer particle to drug cluster size ratio [27] may increase drug cluster interconnectivity. We hypothesized that by increasing the eccentricity of the drug clusters and increasing the polymer particle to drug cluster size ratio in a drug-incorporated polymer matrix, interconnectivity of drug clusters could be reached at lower drug content, thus improving the mechanical properties of the polymer matrix. We demonstrate application of this concept to UHMWPE to develop a load-bearing implant for the treatment of PJI.

Effect of drug cluster eccentricity on elution and strength

A comparison of drug elution rate and tensile mechanical properties was made for low density polyethylene (LDPE), which could be prepared using solvent casting which results in conventional spherical drug clusters (Figure 2a, 2g; continuous) and using compression

molding resulting in highly eccentric drug clusters (Figure 2a, 2g; highly eccentric). Variation in the content of the antibiotic drug vancomycin (2 wt %, 6 wt %, and 10 wt %) and the LDPE to vancomycin particle size ratio (6:1, 16:1, and 40:1) showed that the polymer with the highly eccentric drug clusters showed a higher elution rate than that of the one with spherical drug clusters for 6 and 10 wt% drug loading (Figures 2d–f). This was because the percolation threshold was reached at this loading, a much lower concentration than that for the conventional spherical cluster system. The elongation to break (EAB; Figure 2b), and the ultimate tensile strength (UTS; Figure 2c) were the highest at a polymer to drug particle size ratio of 4:1.

Highly eccentric drug clusters UHMWPE and comparison to BC

Antibiotic-eluting UHMWPE displaying highly eccentric drug clusters was prepared using compression molding. While drug loading at studied levels increased porosity linearly, percolation threshold was reached at a drug loading between 4 and 6 wt% (Supplementary Figures 1 and 2), also corroborated by a sharp increase in drug elution around 6 wt % (Figure 3a). On the other hand, the ultimate tensile strength decreased linearly from 0 wt % to 10 wt % drug loading (Figure 3b).

We created and utilized an optimization equation to maximize the ultimate tensile strength (UTS), impact strength (IS), and drug elution rate (Eq. 1). Because UTS, IS, and elution rate were variable on different scales, their contributions to the optimization were normalized with their respective maximum values (UTS and IS at 0% drug loading and elution rate by 14 % drug loading).

$$\boldsymbol{Opt\ Eq}: Max\,(0.5 * \%\ UTS\,(C) + 0.5 * \%\ IS\,(C) + (\%\ Rate\,(C,t)) \quad (1)$$

Solving for this equation showed that the optimum drug loading was 7 wt% (Figures 3c). Above this concentration, the additional gain in drug elution rate was offset by the decrease in the mechanical properties, while below this concentration the drug elution rate was not sustained at an effective level for treating PJI.

We compared the drug elution of our optimized polymer system with 11 wt% vancomycin in BC, which is the highest drug content that can still maintain the industry standard of 70 MPa for compressive strength [28]. The vancomycin elution rate and antibacterial activity of 7 wt % vancomycin-loaded UHMWPE (VPE) was similar to that of 11 wt% vancomycin in BC (Figure 3d and Supplementary Figure 3), supporting our hypothesis that the highly eccentric drug clusters resulted in more efficient drug release. Vancomycin elution of VPE and BC in synovial fluid did not show any statistically significant difference than elution in phosphate-buffered saline (PBS) (Supplementary Figure 4).

The mechanical properties (yield strength, UTS, IS, EAB) and wear rate of VPE was all within the limit of clinically used UHMWPE [29] (Figure 3e–f, Supplementary Figure 5–7). and were superior to those of 11 % vancomycin-loaded BC (Figure 3e and 3f).

Relation between drug type and elution rate from drug eluting UHMWPE

We tested nine different antimicrobials (ciprofloxacin HCl, tobramycin, tetracycline HCl, gentamicin, vancomycin HCl, rifampin, teicoplanin, ceftriaxone, and fusidic acid) that spanned different polar surface areas (PSA, (72–663 $Å^2$)) and molecular volumes (MV, (282–1600 $Å^3$)) [30]. The ratio of these values (PSA/MV) was used to normalize polarity by molecular size. In UHMWPE with highly eccentric drug clusters (Supplementary Figure 8), we found that more polar compounds (PSA/MV > 0.3) had a higher elution rate early, but it dropped more rapidly over time compared to non-polar compounds (PSA/MV<0.3) (Supplementary Figure 9). Therefore, drugs with a large polar surface area or small molecular volume (low PSA/MV) can be advantageous in applications that require a potent, short-term release of medication, such as local anesthetics (bupivacaine, lidocaine, ropivacaine) and anti-fibrinolytics (tranexamic acid). On the other hand, drugs with a smaller polar surface area or larger molecular volume (high PSA/MV) can be advantageous in applications that require a less potent initial release, but sustained elution. For example, pertinent to PJI treatment, rifampin is an antimicrobial that is highly effective in the time-dependent eradication of *S. aureus* biofilm ([31]) but is also hepatotoxic at high concentrations. Therefore, sustained and lower concentration drug release can be beneficial for bacterial eradication while minimizing side effects.

Gamma irradiated VPE enhances anti-bacterial properties

Most clinically used prosthetic joints are irradiated either for sterilization (25–40 kGy (kilogray); [32]) or for cross-linking (>50 kGy; [33]). Sterilization dose (~25 kGy) did not affect the UTS, IS, the elution profile or the wear rate (Supplementary Figure 6) as compared to those of unirradiated VPE. High dose irradiation (100 kGy) decreased the UTS, IS and the wear rate (5.4 mg/million cycles (mg/MC)) but did not affect the elution rate (Supplementary Figure 10).

After vancomycin was eluted for six months and no further elution of vancomycin could be detected by liquid chromatography (detection limit = 0.1 ug/ml), 25 and 100-kGy irradiated VPEs showed less bacterial adherence than that of unirradiated VPE (Figure 3g). Immunofluorescence staining of vancomycin showed fluorescence on the surfaces of the irradiated VPEs but not on unirradiated VPE (Figure 3h, Supplementary Figure 11), indicating the presence of vancomycin on the surfaces of the VPE after all elutable drug was released. This suggested that some vancomycin was immobilized in UHMWPE as a result of irradiation, presumably by grafting through its phenolic hydroxyl group [34].

VPE eradicated planktonic *S. aureus* in PJI model

An intra-articular PJI model was created by implanting osteochondral plugs of VPE, non-antibiotic containing UHMWPE, and a commonly used bone cement spacer formulation [35] (contains 8.3 wt% tobramycin sulfate and 2.3 wt% vancomycin HCl, **VTBC**) in the femoral trochlear groove and a titanium (Ti) plug with a porous surface in the tibial plateau of skeletally mature New Zealand white rabbits. All rabbits received two bacterial suspensions ($5×10^7$ CFU/ml each) that were injected in the distal tibial canal as well as the

intra-articular space (Figure 4a, 4b). None of the rabbits received any antibiotics for the duration of the study (3 weeks).

Overall, 60% of VPE and 40 % of VTBC rabbits survived compared to none of the rabbits which received UHMWPE plugs without any antibiotics (Figure 4e). Immediately post-surgery, no difference in gait and joint movement was observed between control, VTBC and VPE groups. However, after several days, the infected knee in control rabbits were more swollen, retracted, and passive than rabbits receiving VTBC and VPE. No mechanical failure including deformation, fracture, delamination or pitting was observed in the retrieved implants. Bioluminescence imaging of the knee joints at the end-point, two-photon live dead imaging (Figure 4d–g, Supplementary Figure 12), and sonication and culturing of joint tissues and implants (Supplementary Figure 13) did not show any bacterial growth on any component for the rabbits implanted with VPE, suggesting complete eradication of bacteria. However, significant amount of live bacteria were found on all rabbits receiving VTBC albeit in lesser amount than control, indicating an ongoing infection in the VTBC group.

Since vancomycin can be toxic [36], the serum vancomycin concentration was determined. No vancomycin was detected systemically in any of the rabbits at any time point (detection limit 10 ng/ml). Kidney function byproducts (creatinine and body urea nitrogen, or BUN) and liver function enzymes (alanine aminotransferase or ALT and alkaline phosphatase or ALP) remained within normal limits for all rabbits in the VPE group for the duration of the study (Supplementary Figure 14). These results confirmed the efficacy of vancomycin eluted from radiation sterilized VPE *in vivo*.

Rifampin and vancomycin-eluting UHMWPE as implant material

In PJI, the bacterial biofilm is often localized at the bone-implant interface, which is difficult to eradicate due to limited antibiotic penetration administered systemically [37]. Combination of rifampin and vancomycin is the state-of-the art against bacterial biofilm [38], and can synergistically act against both gram positive and gram negative bacteria [39]. The synergy reduces the MIC for vancomycin and can hinder the rapid bacterial resistance associated with rifampin alone [40] by tailoring the concentration ratios of vancomycin to rifampin such that the concentration of vancomycin is higher for the duration of the release.

Based on clinical guidelines for vancomycin:rifampin concentration for the treatment of PJI (Supplementary Table 1), incorporation of 2.5:1 vancomycin: rifampin allowed long term maintenance of vancomycin:rifampin elution rate ratio closest to the clinically desired trough ratio (Supplementary Figure 15). We observed that the vancomycin elution rate was consistently higher than the rifampin elution rate for UHMWPE incorporated with 3 wt% rifampin in addition to 7 wt% vancomycin (RVPE; Figure 3d) and vancomycin elution rate from RVPE was significantly higher than that of VPE and BC (Figure 3d). Rifampin and vancomycin elution of VPE and BC in synovial fluid did not show any statistically significant difference than elution in PBS (Supplementary Figure 4). Pre-eluting the RVPE for one year and then exposing it to liquid culture of *S. aureus* still prevented the bacteria from growing, indicating that the antibiotics eluted from RVPE were still above the MIC for this microorganism in biofilm form. Mechanical strength (ultimate tensile strength and

impact strength) and wear rate were within the limit of clinically used UHMWPE (Figure 3f, Supplementary Figure 5–7).

Rifampin and vancomycin-eluting UHMWPE (RVPE) with a total drug concentration of 10 wt% was localized only in the surface, unloaded regions [17] [18] to minimize the effect of the increased drug concentration on the mechanical properties of the potential implant (Figure 1). Our previous work in spatially controlling the morphological properties of UHMWPE by layering different compositions of UHMWPE during compression molding showed integrity at the interface [41].

An *in vitro* simulation of biofilm formation at the bone-implant interface of a joint implant was done by sandwiching bone, titanium and UHMWPE. A bioluminescent *S. aureus* (Xen 29, Perkin Elmer) biofilm was grown on the porous surface of titanium discs for 48 hr. The surfaces were clamped together with the biofilm-laden porous titanium surface in contact with the bone and the non-porous surface in contact with UHMWPE (Figure 5b). The average synovial fluid volume and the size of the femoral component of a knee implant were used to scale down the size of the RVPE, the volume of media, and the bone-titanium interface respectively (Supplementary Table 2). The average biofilm thickness was 25.5 ± 2.2 μm, in agreement with previous reports [42]. The biofilm was completely eradicated in the sandwiches with RVPE by 48 hr (Figure 5c). Two-photon live-dead fluorescence excitation imaging of the Ti beads revealed > 95 % biofilm eradication in the RVPE group within 96hr, while the bacteria viability in the controls remained constantly elevated for 2 weeks (Figure 5d, 5e). These results suggested that the antibiotics eluted from the UHMWPE implant surfaces could reach therapeutic levels at the bone-implant interface.

In an adaptation of the PJI model for infections with planktonic bacteria above, all rabbits received a titanium rod with fully grown bioluminescent *S. aureus* biofilms in the tibial canal (Figure 6a). There was no statistically significant difference in bioluminescence between the three groups (control, VTBC, and RVPE) prior to implantation (Figure 6b). None of the rabbits received any systemic antibiotics for the duration of the study (3 weeks). All control rabbits and 80% of rabbits receiving VTBC expired whereas all rabbits in the RVPE group survived for 3 weeks (Figure 6f). Because live bacteria was found in the joints during the post-mortem analysis (Figure 6c), we suspect that some of the bacteria spread hematogenously and caused sepsis. Immediately post-surgery, no difference in gait and joint movement was observed between control and RVPE groups. However, after several days, the infected knee in control and VTBC rabbits were more swollen, retracted, and passive than rabbits receiving RVPE. No mechanical failure including deformation, fracture, delamination or pitting was in the retrieved implants. No live bacteria was observed in the RVPE group as tested by bioluminescence (Figure 6c, Supplementary Figure 16), two-photon live dead imaging (Figure 6e, and 6g), and sonication with subsequent culturing of joint tissues and implants (Supplementary Figure 17). Kidney function byproducts (creatinine and body urea nitrogen, or BUN) and liver function enzymes (alanine aminotransferase or ALT and alkaline phosphatase or ALP) remained within normal limits for all rabbits in the RVPE group during the duration of the study (Supplementary Figure 18). These results confirmed the efficacy of this potential implant material against a *S. aureus* biofilm *in vivo*.

Because of the potential inhibition of implant fixation due to high dose rifampin [43], we tested the effect of RVPE implants on the bony ongrowth to the surface of metal screws (**Methods**). To create the most clinically relevant model, the ratio of RVPE surface area to the bone-implant interface in the murine model was matched to those in the human knee (Supplementary Table 3). RVPE (n=4) or control UHMWPE (n=4) plugs were implanted in the distal femur while stainless steel screw was implanted on the femur (Supplementary Figure 19a). All rats were euthanized six weeks post implantation. Bony ongrowth to the metal was observed in all rats (Supplementary Figure 19b). No statistically significant difference in bone volume to total volume ratio (BV/TV) of bone surrounding the screw was observed (Supplementary Figure 19c).

Discussion

We report a new method of making a drug eluting polymer with highly eccentric drug clusters. This results in improved mechanical strength, and sustained drug elution at lower drug loading as compared to conventional polymers with spherical drug clusters (Figure 1). The method was applied to both low and high melt flow index polymers (e.g. UHMWPE and LDPE respectively). There is possibility of applying this technique to other commonly used drug eluting polymer systems such as poly(lactic-co-glycolic acid). In addition, the effects of drug chemistry and structure have been studied while maintaining the highly eccentric morphology (Supplementary Figure 4), evaluating the possibility of using this morphology for other drug-polymer combinations to treat various diseases. Due to higher interconnectivity, the highly eccentric drug clusters in polyethylene enabled the reduction of the drug percolation threshold from very high drug loading (40–60%) [23] to 6–8 wt% (Supplementary Figures 1 and 2, Figure 3a). The interconnected morphology also resulted in drug elution sustained for a longer duration (Figure 2d–f) and higher mechanical strength (Figure 2b–c) than those of drug eluting polyethylene with spherical drug clusters. Lower initial drug loading may also imply a higher safety margin in adverse scenarios where incorporated drugs may be unintentionally released.

Polymeric matrices can be effective local delivery devices because they enable more effective drug delivery than through systemic administration; they can also enhance the efficacy of the incorporated drugs by targeting the required location of treatment [44]. Common strategies involve injectable, drug eluting polymers in the form of microspheres [45] or micelles [46], but degradation products can be toxic [47], drug elution rate can fall below effective levels [46], and drug release can have low efficacy [46]. The gold standard for drug-incorporated polymers for treating PJI is antibiotic-eluting BC made of PMMA [13], which can only be used in limited load-bearing applications [48]. A fully load bearing permanent implant using UHMWPE can address the shortcomings of other drug-eluting polymers in joint replacement. This reported highly eccentric drug clusters combined with our spatial controlled consolidation technology can enable the sustained delivery of the state-of-the-art antibiotic combinations without sacrificing from the required mechanical properties of the implant. The combination of UHMWPE’s long track record of safety and efficacy [33] with well-known antibiotics such as vancomycin and rifampin has the potential of eliminating the use of antibiotic-eluting spacers and reducing the gold standard two-stage treatment surgeries for PJI to a single surgery. Based on the effects of increasing antibiotic

concentration on the mechanical properties of UHMWPE and the contact stresses of the joint [49], we proposed several implant designs (Supplementary Table 4). All of the designs provided have mechanical strengths and wear rate within the range of clinically used UHMWPE (conventional UHMWPE and highly-crosslinked UHMWPE (HXLPE) (Supplementary Table 3). The uniform vancomycin-containing UHMWPE (7 wt%; VPE) and VPE with a surface layer of rifampin and vancomycin-containing UHMWPE (10 wt%) are intended for temporary (6–8 weeks) usage or for longer term in patients with low activity because the wear rate was closer to conventional UHMWPE than HXLPE. Virgin UHMWPE with a surface layer of rifampin and vancomycin-containing UHMWPE (10 wt %; RVPE) can be used for long-term (years) because its articulating surface is composed of HXLPE with the lowest wear rate.

In addition to the risk of mechanical failure during weight bearing, antibiotic-eluting PMMA BCs showed bacterial adhesion [50] even during antimicrobial elution [51]. On the other hand, radiation sterilized VPE significantly reduced bacterial adherence through surface-bonded vancomycin (Figure 3g and 3h). This is in agreement with previous reports on vancomycin grafting on titanium preventing biofilm formation on its surface [52]. Reduction of bacterial adherence was shown to reduce the infection rate [53]. Surface-bound vancomycin has been shown to eradicate bacteria by making the peptidoglycan layer essential to biofilm formation less rigid and more permeable. As a result, the osmotic pressure can cause bacterial death [52]. In addition to sustaining effective concentrations of antibiotic elution for bacterial eradication, grafting of the antibiotic by irradiation may further hinder bacterial attachment in antibiotic-eluting UHMWPE in the longer term.

VPE and RVPE outperformed clinically-used antibiotic eluting bone cement VTBC in planktonic and biofilm PJI models, respectively. The ability of VTBC to control the bacterial concentration was better in the planktonic model than that in the biofilm model presumably because bacterial susceptibility to vancomycin and tobramycin decrease by at least 1000 fold in biofilm form [54]. While similar survival rate was observed for animals treated with VPE and VTBC, VPE (but not VTBC) completely eradicated all the bacteria in the joint. This may be partly due to Xen29's higher susceptible to vancomycin [55] than to tobramycin [56].

Usage of antibiotic intravenously, orally, or in the form of antibiotic eluting bone cement, VPE, and RVPE all come with a risk of developing resistant bacteria. It has been shown that even when bacteria was exposed to 200 times its minimum inhibitory concentration (MIC), it can develop resistance within 10 hours [57]. This suggests that our previous understanding that bacterial resistance is directly related to being exposed to below-MIC concentrations of antibiotics [58] may be incomplete. Nevertheless, by matching the vancomycin elution of VPE to clinically used vancomycin eluting bone cement (Figure 3d), we expect VPE to pose no extra risk in bacterial resistance development to antibiotic eluting bone cement. In the case of RVPE, by creating elution of vancomycin that exceeds the antibiotic eluting bone cement (Figure 3d), and by ensuring that vancomycin elution is always higher than that of rifampin to prevent sole exposure of bacteria to rifampin, we also expect that RVPE will not pose any extra risk of bacterial resistance development to antibiotic eluting bone cement.

Loading UHMWPE with therapeutic agents using highly eccentric drug clusters could potentially address problems such as pain, osteolysis, osteoporosis and infection in joint arthroplasty and other orthopaedic fields such as trauma and spine. In addition, the application of this morphology to other drug-polymer matrices could also benefit treatment in other applications where both drug elution and mechanical strength are crucial for the implants' success.

Methods

General experimental approaches

No samples, rabbit, or data points were excluded from the analyses. Samples were not randomized to experimental groups unless specified. Lapine experiments and analyses were not performed in a blinded fashion.

Solvent casting of vancomycin eluting LDPE with spherical drug clusters

LDPE was dissolved slowly in boiling xylene (138°C) to reach concentration of 60 mg/mL. After all LDPE had dissolved in xylene, the resulting solution was then cooled to 110°C. Under mechanical stirring, vancomycin crystals with crystal size < 75 um were added to reach the desired weight percent with respect to the LDPE content (0–10 wt %) and kept at 110°C for 30 minutes to further remove the solvent. Resulting viscous solution was then transferred to a stainless steel rectangular mold (50 by 85 mm) and then put in a vacuum oven with a vacuum pressure of −0.1 MPa at 90°C to further remove the solvents.

Manufacture of vancomycin eluting LDPE with highly eccentric drug clusters

LDPE pellets were cryo-milled and then sieved to the appropriate desired particle size ranges. Vancomycin-HCl was crushed with mortar and pestle and then passed through a 75 um sieve. To create vancomycin eluting LDPE with 7 wt% drug loading, 0.7 gram of the sieved vancomycin powder was mechanically mixed with the 9.3 gram cryo-milled LDPE powder for 30 minutes at room temperature. Resulting mixture was then transferred to rectangular mold with dimension of 50 × 85 mm and compressed at 25°C for 1 minute at 10 MPa. The compressed solid mixture was subsequently heated at −0.1 MPa, 190°C for 30 minutes and then compression molded at 10 MPa for 1 minute then cooled to 25°C at 10°C/min.

Manufacture of optimized vancomycin eluting UHMWPE with highly eccentric drug clusters (VPE)

Vancomycin-HCl (1.75 gram) was crushed with mortar and pestle and then passed through a 75 um sieve. Vancomycin powder was then mechanically mixed with GUR1020 UHMWPE powder (Celanese, 23.25 grams) for 30 minutes at room temperature to obtain a 7 wt% vancomycin-blended UHMWPE and poured to circular mold with 10.5 cm inner diameter. Vancomycin-UHMWPE mixture was then consolidated by compression molding at 170°C, 20 MPa, for 5 minutes. Resulting consolidated VPE was then cooled at rate 10°C/min to room temperature to yield approximately 3 mm-thick and approximately 10.5 cm diameter vancomycin blended-UHMWPE.

Manufacture of optimized rifampin-vancomycin eluting UHMWPE with highly eccentric drug clusters (RVPE)

Rifampin (0.4 gram) was crushed with mortar and pestle and then passed through 75 um sieve. Vancomycin-HCl (0.8 gram) was crushed with mortar and pestle and then passed through a 75 um sieve. Rifampin powder and vancomycin-HCl powders were then mechanically mixed for 30 minutes at room temperature. UHMWPE GUR 1020 (12 gram) was added to the rifampin and vancomycin-HCl mixture and mechanically mixed/blended for 30 minutes at room temperature, obtaining a 3 wt% rifampin and 7 wt% vancomycin-blended UHMWPE. 10 grams of the resulting rifampin and vancomycin-blended UHMWPE were transferred and spread evenly onto circular stainless steel mold with inner diameter of 11 cm. 25 grams of GUR 1020 UHMWPE without additives were then added and spread evenly on top of the rifampin and vancomycin-blended UHMWPE. Resulting constructs was then consolidated by compression molding at 170°C, 20 MPa, for 5 minutes and then cooled at rate 10°C/min to room temperature.

Manufacture of vancomycin eluting PMMA bone cement

Vancomycin-HCL powder that had been crushed with mortar and pestle and passed through at 75 um sieve was then mechanically mixed with PMMA powder (Simplex P, Stryker) for 30 minutes at room temperature. After thorough mixing, the cement's liquid monomer was added and then mixed thoroughly with spatula. The vancomycin-cement dough was then poured into stainless steel mold to form its final shape. After about 15 minutes, the hardened vancomycin eluting PMMA bone cement was removed from the mold.

Manufacture of clinically relevant PMMA bone cement spacer (VTBC)

Tobramycin sulfate (3.6 gram) and vancomycin HCL powder (1 gram) that had been crushed with mortar and pestle and passed through at 75 um sieve was then mechanically mixed with PMMA powder (30 gram, Simplex P, Stryker) for 30 minutes at room temperature. After thorough mixing, the cement's liquid monomer was added and then mixed thoroughly with spatula. The antibiotic containing-cement dough was then poured into stainless steel mold to form its final shape. After about 15 minutes, the hardened VTBC was removed from the mold. VTBC samples were ethylene oxide sterilized prior to implantation.

In-vitro drug release from drug eluting UHMWPE and drug eluting PMMA bone cement

For drug eluting UHMWPE, blocks with dimension of 5 mm × 5 mm × 20 mm (n=6) were cut from the consolidated samples. For drug eluting PMMA bone cement, vancomycin-cement dough was poured into stainless steel mold to form 5 mm × 5 mm × 20 mm. Each block was immersed in 1 ml of phosphate-buffered saline at 37°C for a pre-determined time points (6 hr, 24 hr, every 24 hr until 1wk, and then once every week up to a total period of 12 months. After each time-point was reached, the specimens were washed with phosphate-buffered saline and placed in a new 1 ml of phosphate-buffered saline. Concentrations of vancomycin and rifampin were determined using Ultraviolet-Visible spectroscopy (UV-Vis) at 280 nm (vancomycin) and 450 nm (rifampin). Rate of drug release was calculated by dividing the measured concentration with the duration the sample was contacted with phosphate-buffered saline.

Scanning Electron Microscopy

All LDPE, UHMWPE, and PMMA bone cement were sputter coated with a thin layer of gold/palladium and imaged on a Zeiss Supra55VP microscope. Both Everhart-Thronley and Inlens detector were used to acquire the image.

Structural analysis of drug eluting UHMWPE with highly eccentric drug clusters using micro-CT

Tomograms of cylindrical pins (9 mm diameter and 5 mm long) were acquired and reconstruction using cone-beam X-ray scanner (μCT 40, Scanco Medical) for 3D reconstruction with voxel resolution of ~10 um. Porosity analysis and pore accessibility were analyzed using iMorph software package (www.imorph.fr; [68]). Resulting tomogram was then thresholded to partition between the pores and the polymeric matrix. Porosity was calculated by dividing the volume belonging to the pore to the total volume of the samples. The accessible porosity module implanted in iMorph allowed quantification of the pore volume accessible from one side of the sample by a particle depending on its size.

Tensile strength measurement

Type V samples (n=5 for each group) were stamped out of 3.2 mm thin sections of the materials mentioned above according to ASTM-D638. These samples were tested in tension (Insight™, Prairie, MN) with a crosshead speed of 10mm/min. The stress and strain were recorded at 100Hz and the gauge length was monitored using a laser extensometer. The engineering stress-strain curves were calculated by using the crosshead displacement. The ultimate tensile strength (UTS), yield strength (YS), elongation at break (EAB), work to failure (WF), and Young's modulus (E) were calculated.

Fracture toughness measurement

Samples with dimensions of 63.5×12.7×6.35 mm^3 (n=5) were double notched according to ASTM D256 and were impact fractured with a hammer (CEAST Instron). The energy loss of the pendulum after impacting was recorded as the impact strength of the samples.

Determination of wear rate by bi-directional pin-on-disc (POD) test

Cylindrical pins (9-mm diameter and 13-mm long, n=3 each) were machined using CNC mill (ShopBot) from the materials prepared above. The pins were wear tested with a rectangular pattern (5 × 10 mm) against polished CoCr discs at 2Hz in undiluted, preserved bovine serum as a lubricant. The pins were cleaned and weighed before testing and at each 0.16 million cycles (MC) after the first 0.5 MC until a total of 1.2 MC. The wear rate was determined by a linear regression of the weight loss as a function of number of cycles from 0.5 to 1.2 MC.

Antibacterial activity of VPE and vancomycin eluting PMMA bone cement

Relative antibacterial activity of VPE and bone cement was assayed using protocol modified from previously reported [69]. Cylindrical discs (8 mm diameter and 3 mm thick) of VPE and vancomycin eluting PMMA bone cement were sterilized using ethylene oxide. Test organisms (*Staphylococcus aureus* (ATCC 29213) or *Staphylococcus epidermidis* (ATCC

35984)) were cultured in tryptic soy broth at 37°C for 24 hr and subsequently plated to Mueller-Hinton agar at 37°C for 18 hr. Three to five colonies were then selected and suspended in Mueller-Hinton broth and the inoculum concentration was adjusted to 0.5 McFarland turbidity standards. Surface of new Mueller-Hinton agar plate was then covered uniformly with bacteria suspension using sterile swab. Samples were then placed on the surface of the Mueller-Hinton agar plates that had been seeded with either the *S. aureus* or *S. epidermidis* strains and further incubated at 37°C for 24 hr. Pictures of the back of the plates and a ruler were taken. Area of inhibition (clear area where there is no sign of bacterial growth) was then measured using Image J software. When bacteria grow to the immediate surrounding of the implants, the inhibitory area is 3.14*4*4 =50.24 mm^2. Samples were then transferred to new Mueller-Hinton agar plates that had been seeded with either *S. aureus* or *S. epidermidis*. These steps were repeated every 24 hour until three weeks were reached.

Determination of vancomycin grafting on gamma beam irradiated UHMWPE

VPE, RVPE and UHMWPE with no antibiotics (control) were incubated in PBS for 12 months. PBS was replaced every week until the end of study. At 12 months, no vancomycin and rifampin could be detected by both UV-Vis and HPLC. Samples were then washed twice with PBS and blocked for 30 min using 10% fetal bovine serum in distilled, deionized water (blocking buffer). Samples were then incubated with mouse anti-VAN IgM (1:300; U.S. Biologicals, Swampscott, MA) in blocking buffer at 4°C for 12 hr, washed with PBS, and incubated with AlexaFluor 488-coupled goat anti-mouse IgM (A-21042, Thermo Fisher Scientific) diluted 1:300 in blocking buffer at room temperature for 1 hr. Samples were then washed three times in PBS, followed by 2×30 min incubations in PBS. Particles were then visualized using inverted fluorescence microscope (Nikon Eclipse TE2000).

Antibacterial activity of surface-bonded vancomycin on gamma irradiated UHMWPE

VPE, RVPE and UHMWPE with no antibiotics (control) were incubated in PBS for 12 months. PBS was replaced every week until the end of study. At 12 months, no vancomycin and rifampin could be detected by both UV-Vis and HPLC. Samples were then washed in PBS and sterilized by ethylene oxide and then incubated in 1 ml of 1 % dextrose/PBS. *S. aureus* (ATCC 29213) was cultured in trypticase soy broth for 12 hr. The culture was pelleted by centrifugation at 3200 × g for 5 min, and then resuspended in Mueller-Hinton broth to create 1.5×10^8cfu/ml using 0.5 McFarland standard. Two microliter of the bacterial suspension is added to each well and the cultures were incubated at 37°C for 12 hr. Samples were then washed twice with PBS to remove planktonic bacteria. Samples were then stained using Live/Dead BacLight Viability kit (Molecular Probes) that contain Syto 9 and propidium iodide. Samples were then imaged using inverted fluorescence microscope (Nikon Eclipse TE2000), where live bacteria showed green fluorescence, while dead bacteria showed red fluorescence.

Two-photon fluorescence microscopy

For quantification of antibacterial activity, a home-built, two-photon fluorescence microscope was employed to image samples stained with Live/Dead BacLight Viability kit (Molecular Probes). The system includes a mode-locked Ti:Sapphire Laser (MaiTai DeepSee eHP, Newport), providing light at ~150fs pulse width at 80 MHz repetition rate.

The emitted light was detected by two photomultiplier tubes through appropriate dichroic and bandpass filters for Syto9 and propidium iodide. A 10x, 0.3 NA objective (Leica) was used for visualization of multiple beads in one field-of-view (FOV at 10x~ 600 × 600 μm^2), while a 40x, 0.6 NA objective (Nikon) was used for quantification of live/dead bacteria fluorescence. At least 5 images randomly selected throughout the sample were taken for each sample for data quantification.

Antibacterial activity of RVPE on biofilm in between bone-titanium interface

RVPE created as mentioned above was machined into discs (5 mm diameter). The following were also used: (1) a 4 mm-thick consolidated UHMWPE without additives (control), which was prepared using the same molding conditions and (2) titanium discs coated with titanium discs (10 mm diameter, 5 mm thickness, bead diameter 100μm. Manufactured by Orchid Orthopedics, Memphis, TN, USA) and (3) bovine cortical bone discs (10 mm diameter, 3 mm thickness. Bovine cortical bone is machined from bovine tibia obtained from Animal Technology, Texas, USA). All samples were sterilized with ethylene oxide gas. Fresh overnight liquid culture of Bioluminescent *S. aureus* (Xen 29, Perkin Elmer) was diluted to 5 × 10^4 cfu/ml. 50 uL of the liquid culture was added on top of the beaded-surface of the titanium discs to simulate an infection at an orthopaedic implant-bone interface. Cortical bone was added on top of the titanium disc seeded with bacteria and held together with the circular clamp (McMaster-Carr). The constructs were then immersed in 5 ml of fresh Mueller-Hinton II broth and then incubated at 37°C for 48 hr. After 48 hr of incubation, the media was aspirated, clamps were removed, and titanium discs and cortical bone were separated and washed with PBS to remove planktonic bacteria. Biofilm formation was then measured using a bioluminescence camera (IVIS 100, Perkin-Elmer). Cortical bone was placed back on top of the titanium after imaging and either control UHMWPE or RVPE were added underneath the titanium-bone constructs and then clamped using sterile clamps. Samples were then separately placed in its own well in a 6-well plate and 5 ml of Mueller-Hinton II broth was added to each well. All samples were then incubated at 37°C. Bioluminescence was measured at 24 hr, 48 hr, 96 hr, 120 hr, 1 wk, and 2 wk after exposure to either control or RVPE. During each bioluminescence measurement, media was aspirated, clamps were removed, titanium discs and cortical bone were separated and washed with PBS to remove planktonic bacteria, and titanium discs and cortical bone were imaged separately. After imaging, constructs were reassembled, new sterile clamps were placed, and new Mueller-Hinton media was added. Media was replaced every 24 hr. After the samples reached the predetermined time point, samples were then stained using Live/Dead BacLight Viability kit (Molecular Probes) that contain Syto 9 and propidium iodide. Samples were then imaged using two-photon fluorescence microscopy where live bacteria showed green fluorescence, while dead bacteria showed red fluorescence. Percent red fluorescence, corresponding to percent cell death was calculated using Matlab by dividing the number of detected red pixels by the total number of fluorescent pixels.

Lapine planktonic bacteria prosthetic joint infection model

Study approval was granted from Pine Acres Research Facility Institutional Animal Care and Use Committee (protocol 15–06, Norton, MA). Based on the pilot *in vivo* mice study, the standard deviation in total flux from bioluminescence is 200,000 p/s. Taking type I error

of 5 % and 80% power, to detect mean difference of total bioluminescent flux between control and treatment groups of 370,000 p/s, sample size of at least 4.6 was needed per group. A total of ten fully immune-competent, skeletally mature male New Zealand rabbits aged 12 months were used in this study. Animals were randomly assigned to control (non-antibiotic eluting UHMWPE) or VPE groups (7 wt% vancomycin-blended UHMWPE). Each rabbit in the control group received two UHMWPE-only implants (3 mm diameter × 6 mm in height) in the patellofemoral groove, and one beaded titanium rod in the tibial canal (4 mm diameter × 12 mm length). Each rabbit in the VPE group received two VPE implants (same dimensions as control) in the patellofemoral groove and one beaded titanium rod in the tibial canal (same dimensions as control).

Anesthesia was achieved using intramuscular ketamine-xylazine (40 mg/kg-5 mg/kg IM) and inhaled isoflurane (1.5–2.5 %) supplemented with oxygen (1.2 liter/min). Pre-emptive analgesia was administered 30 minutes before the procedure started (buprenorphine 0.02–0.05 mg/kg SC). No pre or postoperative antibiotics were administered. The rabbits were placed in the supine position and the right or left leg was prepped and draped in a sterile fashion (randomization of operated leg established using random.org). A parapatellar incision was performed, the joint capsule was incised, the patella was displaced, and two osteochondral defects were created in the trochlear groove (2.9 mm diameter × 6 mm depth). No antibiotic polyethylene implants (control branch) or VPE (VPE branches) implants were press-fitted into the defects. For the titanium implant, the tibial plateau accessed, and a defect was created by drilling distally into the marrow, creating a 3.9 mm diameter and 12 mm depth defect. 5×10^7 cfu of bioluminescent *Staphylococcus aureus* (Xen 29, Perkin Elmer) in 50 uL 0.9 % saline was injected into the tibial defect, followed by press-fitting the titanium implant, sealing the bacteria *in situ*. The patella was than relocated onto the trochlear groove and soft tissues were approximated using sutures. An additional dose of 5×10^7 cfu of bioluminescent *Staphylococcus aureus* (Xen 29, Perkin Elmer) in 50 uL 0.9 % saline was injected into the knee. All animals received buprenorphine 0.02–0.05 mg/kg SC q12 h throughout the study. After recovering from anesthesia, rabbits were housed individually in cages (22″x25″x26″). Load bearing on implants was allowed immediately after surgery, as no postoperative limiting motion device was utilized. Twice a day, rabbits were removed from their cages and placed in an open space to visually inspect the operated joint and gait. All animals were monitored at least twice throughout the study. Complete blood count (CBC) and chemistry (vancomycin, creatinine, BUN, ALT, and ALP) were assessed before surgery, post-operative day 3, day 7, day 14, and day 21.

Post-mortem bioluminescence imaging was performed on all operated knees (a midline incision was performed on the knee and the joint capsule was opened to expose the joint space). Bioluminescence signal was measured whenever the rabbits expired, or when the study endpoint was reached (day 21). After imaging, the knees were dissected to aseptically isolate the femur, quadriceps tendon (including patella and patellar tendon), tibia, titanium and UHMWPE implants. The titanium rods were stained with BacLight® Bacterial Live-Dead Stain and imaged using two-photon fluorescence microscopy to detect presence of live bacteria. The femur, quadriceps tendon, tibia, and UHMWPE implants were separately sonicated in sterile saline; saline was then cultured in Mueller-Hinton II broth at 37°C for 24 hr to detect presence of live bacteria.

Lapine biofilm bacteria prosthetic joint infection model

Based on the pilot in vivo mice study, the standard deviation in total flux from bioluminescence is 200,000 p/s. Taking type I error of 5 % and 80% power, to detect mean difference of total bioluminescent flux between control and treatment groups of 370,000 p/s, sample size of at least 4.6 is needed per group. Ten rabbits were randomly assigned to control (non-antibiotic eluting UHMWPE) or RVPE groups (layered 6.7 wt % vancomycin and 3.3 wt % rifampin in UHMWPE and non-antibiotic UHMWPE). Each rabbit in the control group received two UHMWPE cylinders without additives (each 3 mm in diameter and 6 mm in length) in the patellofemoral groove, and one beaded titanium rod covered with Xen 29 *S. aureus* biofilm in the tibial canal (4 mm diameter and 12 mm in length). Each rabbit in the RVPE group received two RVPE implants (each 3 mm in diameter and 6 mm in length) in the patellofemoral groove and one beaded titanium implant covered with Xen 29 *S. aureus* biofilm in the tibial canal (4 mm diameter and 12 mm in length).

To create the Xen 29 *S. aureus* biofilm covered titanium rod, fresh overnight liquid culture of Bioluminescent *S. aureus* (Xen 29) was diluted to 5×10^4 cfu/ml. 50 uL of the liquid culture was then added to the 2 ml Mueller-Hinton II broth. Sterile titanium rod was then immersed in the bacterial suspension and incubated at 37°C for 48 hr. Titanium rods were then washed with PBS twice and then imaged with bioluminescent imaging to ensure uniform biofilm formation on all of the samples. One titanium rod was sacrificed for measurement of biofilm thickness using samples were then stained using Live/Dead BacLight Viability kit (Molecular Probes) that contain Cyto 9 and propidium iodide and imaged using two-photon fluorescence microscopy.

Anesthesia was achieved using intramuscular ketamine-xylazine (40 mg/kg-5 mg/kg) and inhaled isoflurane (1.5–2.5 %) supplemented with oxygen (1.2 liter/min). Pre-emptive analgesia was administered before the procedure started (buprenorphine 0.02 mg/kg). No pre or postoperative antibiotics were administered. The rabbits were placed in the supine position and the right or left leg was prepped and draped in a sterile fashion (randomization of operated leg established using random.org). A parapatellar incision was performed, the joint capsule was incised, the patella was displaced, and two osteochondral defects were created in the trochlear groove (2.9 mm diameter × 6 mm depth). Control (for control branches) or VPE (for VPE branches) implants were press-fitted into the defects. For the titanium implant, the tibial plateau accessed, and a defect was created by drilling distally into the marrow, creating a 3.9 mm diameter and 12 mm depth defect. The biofilm-laden titanium implant was then press-fitted into the tibial canal. Load bearing on implants was allowed immediately after surgery, as no postoperative limiting motion device was utilized. Twice a day, rabbits were removed from their cages and placed in an open space to visually inspect the operated joint and gait. All animals were monitored at least twice per day for 3 days following surgery and at least once per day for the remainder of the study. Complete blood count (CBC) and chemistry (vancomycin, creatinine, BUN, ALT, and ALP) were assessed before surgery, post-operative day 3, day 7, day 14, and day 21.

Post-mortem bioluminescence imaging, tissues and implant sonication were performed as described above.

Murine osseointegration model

Based on the pilot *in vivo* rat study, the standard deviation in bone volume/total volume (BV/TV) is 15 %. Taking type I error of 5 % and 80% power, to detect a mean difference of BV/TV between control and treatment groups of 23 %, a sample size of at least 4 rats was needed per group. Eight Sprague-Dawley rats aged 8 weeks were randomly assigned into either control (non-antibiotic eluting UHMWPE) or RVPE (layered 6.7 wt % vancomycin and 3.3 wt % rifampin in UHMWPE and non-antibiotic UHMWPE) groups. Each rat in the control group received an UHMWPE implant without antibiotics (each 3 mm in diameter and 4 mm in length) transcondylarly in the medial distal femur, and one stainless steel screw (3.5 mm in diameter and 5 mm in length) in the tibial canal between the intercondylar eminence.

Anesthesia was achieved using inhaled isoflurane (1.5–2.5 %) supplemented with oxygen (1.2 liter/min). Pre-emptive analgesia was administered before the procedure started (buprenorphine 0.02 mg/kg). No pre or postoperative antibiotics were administered. The rats were placed in the supine position and the right or left leg was prepped and draped in a sterile fashion (randomization of operated leg established using random.org). A parapatellar incision was performed, the joint capsule was incised, the patella was displaced, and a transcondylar defect on the medial distal femoral condyle was created. Control or RVPE implants were press-fitted into the defects. For the stainless steel screw implantation, the tibial plateau was accessed, and a defect was created by drilling distally into the marrow canal. The biofilm-laden titanium implant was then screwed into the tibial canal. Load bearing on implants was allowed immediately after surgery, as no postoperative limiting motion device was utilized. Twice a day, rats were removed from their cages and placed in an open space to visually inspect the operated joint and gait. All animals were monitored at least twice per day for 3 days following surgery and at least once per day for the remainder of the study up to six weeks.

After the rats were euthanized using CO_2, the operated femur and tibia were obtained and soft tissues were removed carefully. The tibia were scanned with micro-CT (Scanco Medical, μCT 40) to give 8 μm resolution at all 3 directions. Three dimensional (3D) image reconstructions were generated using Avizo software (FEI, Oregon, USA). Bone volume (BV) relative to the total volume (TV) was determined by creating a region of interest (ROI) in the shape of 3D cylinder (5 mm diameter, 3 mm height) along the long axis of the screw and centered on the long axis of the screw. Three mm height was chosen as thickness to allow quantification consistently on the epiphysis region. The same ROI was used for all samples. The 3D images were thresholded to differentiate hard tissue (bone), screw, and soft tissue-empty space. BV was calculated from the volume of the bone, and TV was calculated as the total volume of bone+soft tissue-empty space.

Statistical analysis

All statistical tests were performed by Student’s two-tailed t-test for comparison of two groups and analysis of variance (ANOVA) for comparisons of multiple groups implemented through software package GraphPad Prism version 4.0. All error bars used in this report are mean ±s.d. of at least three independent experiments except the lapine study (single

experiment). Survival analyses were performed by using a log-rank test, using a statistical software package GraphPad Prism version 4.0. All data are mean ± s.d., combined from three independent experiments.

Data availability

The authors declare that all data supporting the findings of this study are available within the paper and its supplementary information.

Supplementary Material

Refer to Web version on PubMed Central for supplementary material.

Acknowledgments

We are grateful to Gregory Wojkiewicz and Benoit Tricot of Center for Systems Biology, MGH for assistance with the bioluminescence imaging. This work was performed in part at the Center for Nanoscale Systems (CNS), a member of the National Nanotechnology Infrastructure Network (NNN), which is supported by the National Science Foundation under NSF award no. ECS-0335765. CNS is part of Harvard University. This study was supported in part by Harris Orthopedics Lab Sundry Fund, MGH Orthopedics Departmental Fund, US National Institutes of Health grants P01-HL120839 and P41-EB015903.

References

1. CDC/NCHS. National Hospital Discharge Survey. 2010.
2. Paxton EW, Inacio M, Slipchenko T, Fithian DC. The Kaiser Permanente National Total Joint Replacement Registry. Perm J. 2008; 12:12–16. [PubMed: 21331204]
3. Australian Orthopaedic Association. 2015 Annual Report on National Joint Replacement Registry. 2015 Fig KT29.
4. Kurtz SM, Lau E, Watson H, Schmier JK, Parvizi J. Economic burden of periprosthetic joint infection in the United States. J Arthroplasty. 2012; 27:61–65. [PubMed: 22554729]
5. Kubista B, et al. Reinfection after two-stage revision for periprosthetic infection of total knee arthroplasty. Int Orthop. 2012; 36:65–71. [PubMed: 21553042]
6. Lentino JR. Prosthetic joint infections: bane of orthopedists, challenge for infectious disease specialists. Clin Infect Dis. 2003; 36:1157–1161. [PubMed: 12715311]
7. Segawa H, Tsukuyama DT, Kyle RF, Becker DA, Gustilo RB. Infection After Total Knee Arthroplasty. A Retrospective Study of the Treatment of Eighty-One Infections. J Bone Joint Surg Am. 1999; 81:1434–1445. [PubMed: 10535593]
8. Spellberg B, Lipsky BA. Systemic Antibiotic Therapy for Chronic Osteomyelitis in Adults. Clinical Infectious Disease. 2012; 54:393–407.
9. Pioletti DP, et al. Orthopedic Implant Used as Drug Delivery System: Clinical Situation and State of Research. Current Drug Delivery. 2008; 5:59–63. [PubMed: 18220552]
10. Duncan CP, Masri BA. The role of antibiotic-loaded cement in the treatment of an infection after a hip replacement. Instr Course Lec. 1995; 44:305–313.
11. Radin S, Campbell JT, Ducheyne P, Cuckler JM. Calcium phosphate ceramic coatings as carriers of vancomycin. Biomaterials. 1997; 18:777. [PubMed: 9177855]
12. Lin SS, et al. Development of a biodegradable antibiotic delivery system. Clin Orthop Relat Res. 1999; 362:240–250.
13. Burnett RS, Kelly M, Hanssen AD, Barrack RL. Technique and timing of two-stage exchange for infection in TKA. Clin Orthop Relat Res. 2007; 464:164–178. [PubMed: 17975376]
14. Jung J, Schmid NV, Kelm J, Schmitt E, Anagnostakos K. Complications after spacer implantation in the treatment of hip joint infections. International Journal of Medical Sciences. 2009; 6:265–273. [PubMed: 19834592]

15. Kuhn, KD. Bone Cements: Up-to-Date Comparison of Physical and Chemical Properties of Commercial Materials. Berlin Springer-Verlag; Berlin: 2000. p. 89-93.
16. Lee, C. The Well-Cemented Total Hip Arthropalsty: Theory and Practice. Springer Medizin Verlag; Berlin: 2005. The Mechanical Properties of PMMA Bone Cement; p. 60-66.
17. Cho CH, et al. Elasto-plastic contact analysis of fatigue wear behaviour of UHMWPE tibial ocmponents. Japan J Clin Biomech. 2002; 23:373–379.
18. Korhonen RK, Kostinen A, Konttinen YT, Santavirta SS, Lapallainen R. The effect of geometry and abduction angle on the stresses in cemented UHMWPE acetabular cups – finite element simulations and experimental tests. BioMedical Engineering Online. 2005; 4:32. [PubMed: 15904521]
19. Lilikakis A, Sutcliffe MPF. The effect of vancomycin addition to the compression strength of antibiotic-loaded bone cements. Int Orthop. 2009; 33:815–819. [PubMed: 18283457]
20. Meyer J, Piller G, Spiegel CA, Hetzel S, Squire M. Vacuum-Mixing Significantly Changes Antibiotic Elution Characteristics of Commercially Available Antibiotic-Impregnated Bone Cements. J Bone Joint Surg Am. 2011; 93:2049–2056. [PubMed: 22262375]
21. Thomes B, Murray P, Bouchier-Hayes D. Development of resistant strains of Staphylococcus epidermidis on gentamicin-laoded bone cement in vivo. J Bone Joint Surg Br. 2002; 84:758–760. [PubMed: 12188500]
22. Xie Z, et al. Gentamicin-Loaded Borate Bioactive Glass Eradicats Osteomyelitis Due to Escherichia coli in a Rabbit Model. Antimicrob Agents Chemother. 2013; 57:3293–3298. [PubMed: 23629702]
23. Fan JB, Huang C, Jiang L, Wang S. Nanoporous microspheres: from controllable synthesis to healthcare applications. J Materials Chemistry B, 2013. 2013; 1:2222–2235.
24. Bawa R, Siegel R, Marasca B, Karel M, Langer RS. An explanation for the controlled release of macromolecules from polymers. J Controlled Release. 1985; 1:259–268.
25. Guo QH, Guo S, Wang ZM. Estimation of 5-fluorouracil-loaded ethylene-vinyl acetate stent coating based on percolation threshold. Int J Pharmaceutics. 2007; 333:95–102.
26. Yi YB, Sastry AM. Analytical approximation of the percolation threshold for overlapping ellipsoids of revolution. Proc R Soc Lond A. 2004; 460:2353–2380.
27. Plumlee KP, Schwartz CJ. Development of Porous UHMWPE Morphologies for Fixation of Gel-Based Materials. Journal of Applied Polymer Science. 2009; 114:2555–2563.
28. Amin TJ, Lamping JW, Hendriks KJ, McIff T. E Increasing the Elution of Vancomycin from High-Dose Antibiotic-Loaded Bone Cement: A Novel Preparation Technique. J Bone Joint Surg Am. 2012; 94:1946–1951. [PubMed: 23014891]
29. Collier JP, et al. Comparison of Cross-Linked Polyethylene Materials for Orthopaedic Applications. Clinical Orthopaedics and Related Research. 2003; 414:289–304.
30. Ertl P, Rohde B, Selzer P. Fast Calculation of Molecular Polar Surface Area as a Sum of Fragment-Based Contributions and Its Application to the Prediction of Drug Transport Properties. J Med Chem. 2000; 43:3714–3717. [PubMed: 11020286]
31. Laverty G, Alkawareek MY, Gilmore BF. The In Vitro Susceptibility of Biofilm Forming Medical Device Related Pathogens to Conventional Antibiotics. Dataset Papers in Science. 2014; 2014:1–10.
32. Goldman M, Gronsky R, Pruitt L. The influence of sterilization technique and ageing on the structure and morphology of medical-grade ultrahigh molecular weight polyethylene. Journal of Materials Science: Materials in Medicine. 1998; 9:207–212. [PubMed: 15348894]
33. Kurtz, A., Patel, JD. The Clinical Perfomrance of Highlt Cross-linked UHMWPE in *Hip Replacements*. In: KS, editor. UHMWPE Biomaterials Handbook. Vol. 2016. Elsevier; Waltham: 2016. p. 57-71.
34. Besemer, DC., et al. Evidenve of Vitamine E Grafting to Polyethylene. ORS 2013 Annual Meeting; 2013. Poster 1055
35. Cui Q, Mihalko WM, Shields JS, Ries M, Saleh KJ. Antibiotic-Impregnated Cement Spacers for the Treatment of Infection Associated with Total Hip or Knee Arthroplasty. J Bone Joint Surg Am. 2007; 89:871–882. [PubMed: 17403814]

36. Mellor JA, Kingdom J, Cafferkey M, Keane CT. Vancomycin toxicity: a prospective study. J Antimicrob Chemother. 1985; 15:773–780. [PubMed: 4030539]
37. Glaudemas AWJM, Galli F, Pacilio M, Signore A. Leukocyte and Bacteria Imaging in Prosthetic Joint Infection. European Cells and Materials. 2013; 25:61–77. [PubMed: 23325539]
38. Rose WE, Poppens PT. Impact of biofilm on the in vitro activity of vancomycin alone and in combination with tigecycline and rifampicin against Staphylococcus aureus. J Antimicrob Chemother. 2008; 63:485–488. [PubMed: 19109338]
39. Yee YC, Kisslinger B, Yu VL, Jin DJ. A mechanism of rifamycin inhibition and resistance in Pseudomonas aeruginoasa. J Antimicrob Chemother. 1996; 38:133–137.
40. Bradley JS, Scheld WM. The challenge of penicillin-resistant Streptococcus pneumoniae meningitis: current antibiotic therapy in the 1990s. Clin Infect Dis. 1997; 24:S213–21. [PubMed: 9126696]
41. Oral E, et al. A surface cross-linked UHMWPE stabilized by vitamin E with low wear and high fatigue strength. Biomaterials. 2010; 31:7051–7060. [PubMed: 20579730]
42. Lauderdale KJ, Malone CL, Boles BR, Morcuende J, Horswill AR. Biofilm dispersal of community-associated methicillin-resistant Staphylococcus aureus on orthopedic implant materia. J Orthop Res. 2010; 28:55–61. [PubMed: 19610092]
43. Isefuku S, Joyner CJ, Simpson AH. Toxic effect of rifampicin on human osteoblast-like cells. J Orthop Res. 2010; 19:950–954.
44. Moses MA, Brem H, Langer R. Advancing the field of drug delivery: Taking aim at cancer. Cancer Cell. 2003; 4:337–341. [PubMed: 14667500]
45. Ambrose CG, et al. Effective treatment of osteomyelitis with biodegradable microspheres in a rabbit model. Clin Orthop Relat Res. 2004; 421:203–299.
46. Surdam JW, Licini DJ, Baynes NT, Arce BR. The use of exparel (liposmal bupivacaine) to manage postoperative pain in unilateral total knee arthroplasty patients. J Arthroplasty. 2015; 30:325–329. [PubMed: 25282071]
47. Meyer F, Wardale J, Best S, Cameron R, Rushton N, Brooks R. Effects of lactic acid and glycolic acid on human osteoblasts: a way to understand PLGA involvement in PLGA/calcium phosphte composite failure. J Orthop Res. 2012; 30:864–871. [PubMed: 22105618]
48. Bohner, M. Designing ceramics for injectable bone graft substitutes. In: Vernon, B., editor. Injectable biomaterials: Science and applications. Woodhead Publishing; Cambridge: 2011. p. 24-39.
49. Hua X, Wang L, Al-Haijar M, Jin Z, Wilcox RK, Fisher J. Experimental validation of finite element modelling of a modular metal-on-polyethylene total hip replacement. Proc J Mech E Part H: J Engineering in Medicine. 2014; 228:682–692.
50. Neut D, et al. Biomaterial-associated infection of gentamicin-loaded PMMA beads in orthopaedic revision surgery. J Antimicrob Chemotherapy. 2001; 47:885–891.
51. van de Belt H, et al. Staphylococcus aureus biofilm formation on different gentamicin-loaded polymethylmethacrylate bone cements. Biomaterials. 2001; 22:1607–1611. [PubMed: 11374461]
52. Antoci V, et al. Vancomycin covalently bonded to titanium alloy prevents bacterial colonization. J Orthop Res. 2007; 25:858–866. [PubMed: 17415753]
53. Stewart S, et al. Vancomycin-Modified Implant Surface Inhibits Biofilm Formation and Supports Bone-Healing in an Infected Osteotomy Model in Sheep. J Bone Joint Surg Am. 2012; 94:1406–1415. [PubMed: 22854994]
54. Castaneda P, McLaren A, Tavaziva G, Overstreet D. Biofilm Antimicrobial Susceptibility Increases With Antimicrobial Exposure Time. Clin Orthop Relat Res. 2016; 474:1659–1664. [PubMed: 26797908]
55. Xiong YQ, et al. Real-Time In Vivo Bioluminescent Imaging for Evaluating the Efficacy of Antibiotics in a Rat Staphylococcus aureus Endocarditis Model. Antimicrob Agents Chemoter. 2005; 49:380–387.
56. Kadurugamuw JL, et al. Rapid Direct Method for Monitoring Antibiotics in a Mouse Model of Bacterial Biofilm Infection. Antimicrob Agents Chemoter. 2003; 47:3130–3137.
57. Zhang Q, et al. Acceleration of emergence of bacterial antibiotic resistance in connected microenvironments. Science. 2011; 333:1764–1767. [PubMed: 21940899]

58. Gullberg E, et al. Selection of resistant bacteria at very low antibiotic concentrations. PLoS Patogens. 2011; 7:e1002158.
59. Van Den Heever DJ, Scheffer C, Erasmus PJ, Dillon EM. Contact stresses in patient – specific unicompartmental knee replacement. Clinical Biomechanics. 2011; 26:159–166. [PubMed: 20950903]
60. Villa T, Migilavacca F, Gastaldi D, Colombo M, Pietrabissa R. Contact stresses and fatigue life in a knee prosthesis: comparison between in vitro measurements and computational simulation. Journal of Biomechanics. 2004; 18:45–53.
61. Wang A, et al. Orientation softening in the deformation and wear of ultra-high polyethylene. Wear. 1997; 203/204:230–241.
62. Kurtz, SM. The clinical performance of historical and conventional UHMWPE in *Hip Replacements*. In: Kurtz, SM., editor. UHMWPE Biomaterials Handbook. Elsevier; Waltham: 2016. p. 45-55.
63. American Joint Replacement Registry. Third AJRR Annial Report on Hip and Knee Arthroplasty Data. 2016:23–24.
64. Pruitt, L. Conventional and Cross-Linked Polyethylene Properties. In: Bellemans, J.Ries, MD.Victor, JMK., Victor, editors. Total Knee Arthroplasty: A Guide to Get Better Performance. Springer; New York: 2005. p. 353-360.
65. Oral E, et al. A Surface Crosslinked UHMWPE Stabilized by Vitamin E with Low Wear and High Fatigue Strength. Biomaterials. 2010; 31:7051–7060. [PubMed: 20579730]
66. Baykal D, et al. Advances in tribological testing of artificial joint biomaterials using multidirectional pin-on-disk testers. Journal of The Mechanical Behavior of Biomedical Materials. 2014; 31:117–134. [PubMed: 23831149]
67. Pruitt, L. Conventional and Cross-Linked Polyethylene Properties. In: Bellemans, J.Ries, MD.Victor, JMK., Victor, editors. Total Knee Arthroplasty: A Guide for Better Performance. Springer-Verlag; Heidelberg: 2004. p. 353-360.
68. Pardo-Alonso S, Vicente J, Solorzano E, Rodriguez-Perez MA, Lehmhus D. Geometrical Tortuosity 3D Calculations in Infiltrated Aluminium Cellular Materials. Procedia Material Science. 2014; 4:145–150.
69. Ortez, JH. Disk Diffusion Testing. In: Coyle, MB., editor. Manual of Antimicrobial Susceptibility Testing. American Society for Microbiology; 2005. p. 39-52.

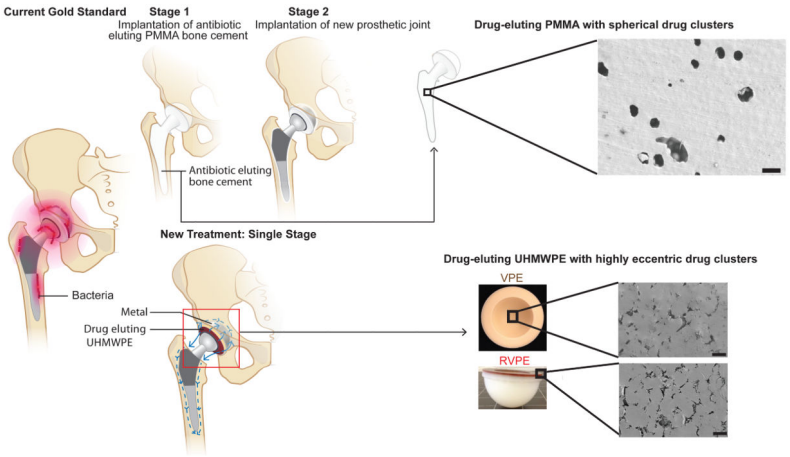

Figure 1. Highly eccentric drug eluting polyethylene

Current gold standard of treatment for prosthetic joint infection (PJI) is two stage surgery, which involves replacement of infected prosthesis with antibiotic eluting PMMA bone cement and intravenous antibiotics (stage 1), and subsequent removal of PMMA bone cement and replacement with a new joint prosthesis after bacterial cultures confirm clearance of infection (stage 2). Because of its spherical drug cluster morphology, PMMA bone cement requires high drug loading for sufficient drug elution and has weak mechanical strength. Drug eluting polyethylene with highly eccentric drug clusters reported in this study allowed much lower drug loading for efficient drug elution, high mechanical strength, and favorable wear rate. Drug eluting PMMA had spherical drug clusters, which require 30–40 % drug content to reach percolation. The high drug loading needed to achieve sufficient drug elution significantly reduces its mechanical strength, to the point of insufficient strength for full load bearing. On the other hand, drug-eluting UHMWPE with highly eccentric drug clusters reached percolation at 6–8 wt % drug content, allowing sufficient drug elution to be reached at lower content than the antibiotic eluting bone cement. As a result, the mechanical strength necessary for a fully functional drug-eluting joint prosthesis is maintained and the direct replacement of infected prosthetic joints with new prosthetic joints without immobilization of patients is possible. All scale bars are 100 μm. VPE= 7 wt % vancomycin in UHMWPE. RVPE= 7 wt % vancomycin + 3 wt % rifampin in UHMWPE (Red) with underlying non-antibiotic eluting (unmodified) UHMWPE (white).

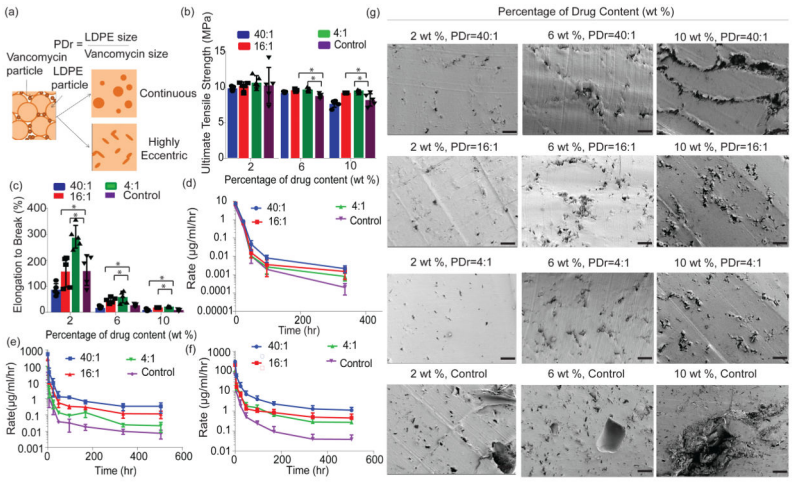

Figure 2. Highly eccentric drug-cluster morphology influences the mechanical and elution properties of the implant material

a, Schematic view of process to create highly eccentric drug clusters in low density polyethylene (LDPE). Vancomycin crystals interspersed between LDPE particles. Subsequent casting or molding under minimum flow to form highly eccentric drug clusters. **b**, ultimate tensile strength and **c**, elongation to break of compression molded LDPE (highly eccentric drug clusters) at various PDr (40:1, 16:1, 4:1) and solvent cast LDPE (traditional spherical drug clusters, control) at different initial drug loading (2, 6, and 10 wt %). **d,e,f** Vancomycin elution rate from both LDPEs at different drug content 2 wt % (**d**), 6 wt % (**e**) and 10 wt % (**f**)). **g**, Scanning electron micrograph (SEM) images of vancomycin eluting LDPE at various initial drug content (2 wt %, 6 wt %, and 10 wt %) and various PDr (40:1, 16:1, 4:1). Scale bar = 100 μm. Also shown is SEM images of vancomycin eluting LDPE made by solvent casting (control). Drugs were pre-eluted before imaging. All data are derived from n=5 (**b–f**) per group. Throughout, data are mean ± s.d., *p<0.05. PDr = Rato of LDPE size to vancomycin particle size. MPa = Megapascal, wt = weight, hr = hour, μg = microgram, ml = mililitre.

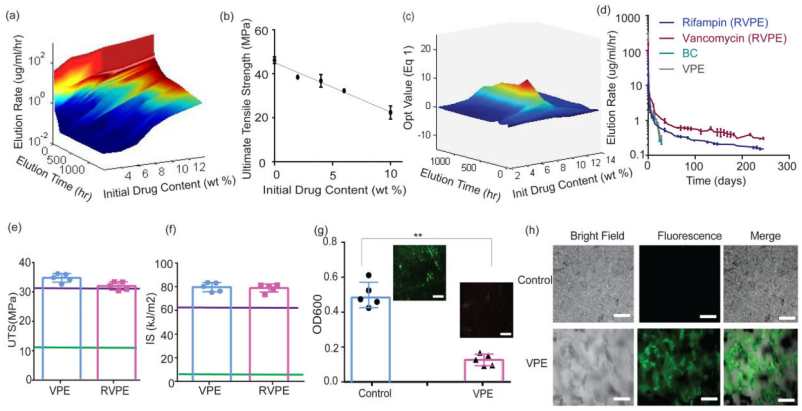

Figure 3. Influence of the highly eccentric morphology of modified UHMWPE on its drug elution and mechanical properties

a, Response surface of vancomycin elution rate, elution time, and initial vancomycin content of highly eccentric morphology in vancomycin eluting ultra-high molecular weight polyethylene. **b**, Relation between ultimate tensile strength and initial drug content. Data are shown as mean ± s.d. (n=5). **c**, Response surface optimization of equation (1) for drug content in UHMWPE and elution time. **d**, Elution rate of RVPE, VPE and bone cement (11 wt % vancomycin loading, BC). Each data point corresponds to mean ± s.d. (n=5). **e,f**, Ultimate tensile strength (UTS) and Impact strength (IS) of VPE and RVPE. Green line indicates the mean value of BC. Purple line indicates the minimum value of clinically used UHMWPE (Collier et al, 2003). Data are shown as mean ± s.d. (n=3). **g**, UHMWPE with no antibiotics (control) and VPE were pre-eluted for six months, then incubated with S. aureus for 24 hours. Adherent bacteria were quantified by sonication and subsequent incubation for 24 hr. Data are shown as mean ± s.d. (n=5), statistical analysis was performed with a two-tailed Student's t-test, **, $p<0.01$. Inset: Adherent bacteria were fluorescently labelled. Green indicates live bacteria, red indicates dead bacteria. Scale bar = 100 μm. **h**, Fluorescence labelling of surface bound vancomycin with mouse-anti vancomycin and fluorescently labelled goat anti-mouse. Samples were pre-eluted for 6 months prior to labelling. Scale bar = 100 μm.

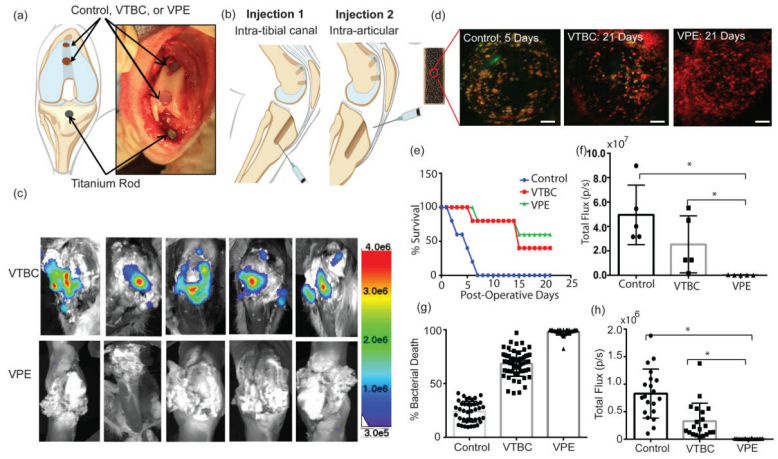

Figure 4. In-vivo evaluation of VPE in joint infection model

a, Schematic and representative gross view of implantation of non-antibiotic eluting-PE (control), VTBC, VPE, and Titanium rod. **b**, Schematic of bacterial injection sites for the two bacterial injection administered to all rabbits in this study. **c**, Bioluminescent imaging of rabbit knee joint with implanted control, VTBC, VPE and titanium rod. Bioluminescent imaging was conducted immediately after each animal either died or was euthanized at the experimental end-point. **d**, Representative two-photon live-dead imaging of adherent bacteria on the explanted titanium. Green indicates live bacteria, red indicates dead bacteria. Scale bar=200 μm. **e**, Survival graph of the rabbit in the control, VTBC, and VPE groups. All controls died within one week, while 40 % of VTBC and 60 % of VPE stayed alive until the end of study. (n=5 per group, $p<0.01$ log rank test). **f**, Total average bioluminescence of the rabbit knees as shown in (**c**). **g**, Mean percentage bacterial death of the bacteria adherent to the surface of titanium rod post-explant. **h**, Average bioluminescence post-sonication and subsequent 12 hr reculturing. Average boluminescence was calculated by averaging total flux for the femur, tibia, implants, patellar tendon, and quadriceps tendon from all rabbits in the same group. (**f–g**) All data are mean ± s.d., statistical tests were performed using student's t-test, *$p<0.05$

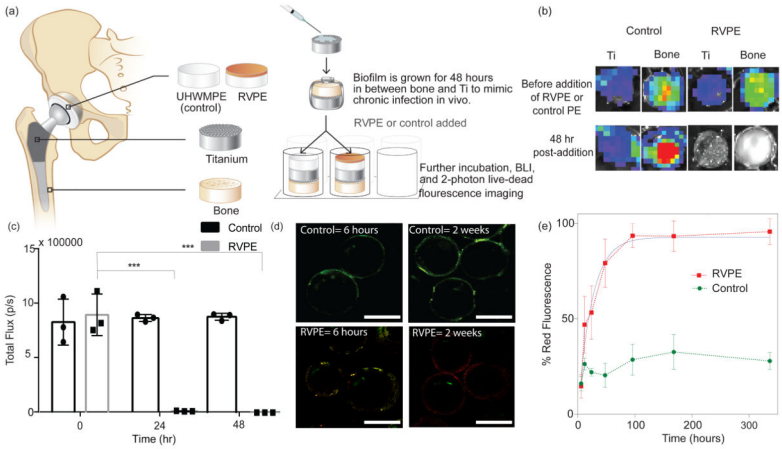

Figure 5. In vitro evaluation of RVPE

a, Schematic of ‘sandwich’ experiment to treat bacterial biofilm in between bone-titanium using either non-antibiotic eluting UHMWPE (control) or RVPE. Bacterial biofilm is often found between titanium and bone surfaces in patients with chronic PJI. Bioluminescence was measured for all 21 constructs. At pre-defined time-points (6 hr, 24 hr, 48 hr, 96 hr, 120 hr, 1 wk, 2 wk, n=3 each for each time point), bone and titanium were live-dead stained and imaged with two-photon fluorescence microscopy. **b,c**, Bioluminescent imaging and its quantification at the Ti-bone interface, after 24 hr and 48 hr treatment with RVPE or control. (n=3, statistical analysis was performed using two way analysis of variance, ***, $p<0.001$). **d**, Two-photon, live-dead imaging of the bacteria that adhered to the surface of titanium at 6 hr and 2 weeks treated with unmodified UHMWPE (control) and RVPE. Scale bar = 200 μm. **e**, Percent live dead as function of time of exposure to either control or RVPE. Data are presented as mean ± s.d.

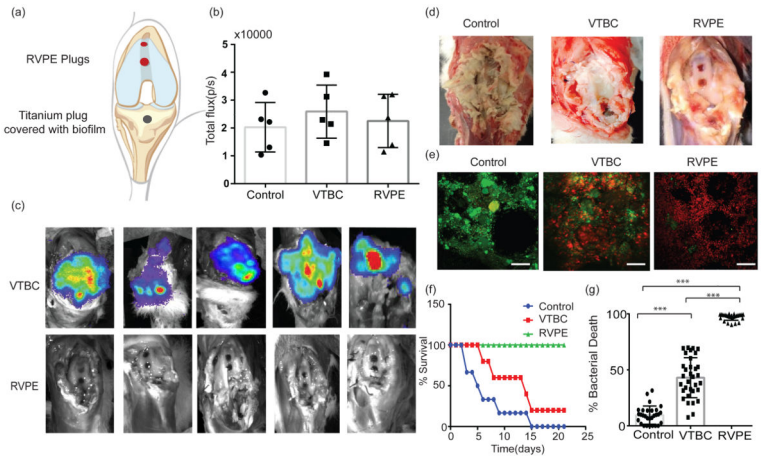

Figure 6. In vivo evaluation of RVPE in a lapine joint Infection model

a, Schematic view of implantation of non-antibiotic eluting UHMWPE (control), VTBC, RVPE, and titanium rod in lapine intraarticular model. **b**, Mean bioluminescence of the titanium rods before implantation in rabbits. **c**, Post-mortem bioluminescent imaging of rabbit knee joints from VTBC and RVPE groups. All rabbits were alive at day 21 in the RVPE treatment. **d**, Representative gross image of a dissected knee from the control, VTBC, and RVPE group. Copious amount of pus was found in the knee joints of the control and VTBC rabbits, whereas no pus was found in the knee joints of the rabbits treated with RVPE. **e**, Representative two-photon live-dead imaging of the bacteria on the titanium rods after retrieval. Green indicates live bacteria, red indicates dead bacteria. Scale bar = 200 um. **f**, Survival graph. None of the control, 20% of VTBC, and 100% of RVPE survived until the end of study. $p<0.01$ comparing control vs RVPE and VTBC vs RVPE by log rank test. g, Mean percent bacterial death of bacteria adherent to titanium rods' surface after retrieval. Data in (b,g) are mean ± s.d. ***$p<0.001$.